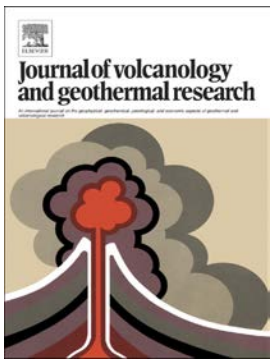

Dynamics of caldera collapse during the Coranzulí eruption (6.6 Ma) (Central Andes, Argentina)

Raúl E. Seggiaro, Silvina R. Guzmán, Joan Martí

PII: S0377-0273(18)30254-3
DOI: https://doi.org/10.1016/j.jvolgeores.2019.02.003
Reference: VOLGEO 6550

To appear in: *Journal of Volcanology and Geothermal Research*

Received date: 28 June 2018
Revised date: 6 February 2019
Accepted date: 9 February 2019

Please cite this article as: R.E. Seggiaro, S.R. Guzmán and J. Martí, Dynamics of caldera collapse during the Coranzulí eruption (6.6 Ma) (Central Andes, Argentina), Journal of Volcanology and Geothermal Research, https://doi.org/10.1016/j.jvolgeores.2019.02.003

Dynamics of caldera collapse during the Coranzulí eruption (6.6 Ma) (Central Andes, Argentina)

Raúl E. Seggiaro [a, b], Silvina R. Guzmán[a*], Joan Martí[c]

[a] Instituto de Bio y Geociencias del NOA (IBIGEO), UNSa, CONICET, 9 de Julio 14, 4405, Rosario de Lerma, Salta, Argentina.

[b] SEGEMAR, Av. Houssay 1099, 4400, Salta, Argentina.

[c] Institute of Earth Sciences Jaume Almera, ICTJA-CSIC, Lluis Sole i Sabaris s/n, 08028, Barcelona, Spain.

* Corresponding author: sguzman@conicet.gov.ar (S. Guzmán)

Abstract

The Coranzulí caldera (23°00' S – 66°15' W) is one of the least known caldera complexes in the eastern part of the Argentinian Altiplano-Puna plateau (Central Andes). It lies at the intersection of N-S, NW-SE and NE-SW fault systems and was formed about 6.6 Ma ago; during the eruption, four main crystal-rich dacitic ignimbrites were emplaced in different directions around the caldera. Caldera collapse was not homogeneous, rather it occurred along different sectors of the ring fault as subsidence progressed. The location of co-ignimbrite lag breccias and the composition of the dominant lithic fragments within the different ignimbrite flow units reveal how the caldera collapse developed. According to the succession of deposits, in particular the lack of an initial fallout and the presence of co-ignimbrite lag breccias associated with the different ignimbrite units, we interpret this caldera-forming eruption as a pulsating boiling-over event in which the caldera collapse developed immediately after the onset of the eruption, favored by a transtensive tectonic system. Within the central part of the caldera, there is Cerro Coranzulí, a resurgent dome that exposes a thick intracaldera ignimbrite succession covered by ~ 100-m-thick dacite lava flows that erupted at the end of caldera formation.

Keywords: Coranzulí; Central Andes; Puna; Altiplano-Puna Volcanic Complex; caldera; crystal-rich ignimbrite

1. Introduction

After Tibet, the Altiplano-Puna is the second largest and second highest plateau in the world (e.g. Allmendinger et al., 1997). This elevated plateau and its magmatism are mainly the result of the subduction of the Nazca plate beneath the South American plate. The Central Volcanic Zone of the Andes extends within the latitudinal segment 16–28°S (e.g. de Silva, 1989) and contains abundant volcanism that has taken place over much of this area since about 26 Ma (Fig. 1). In its central segment lies the Altiplano-Puna Volcanic Complex (APVC: 21–24°S; de Silva, 1989), which has been studied extensively because it contains one of the largest ignimbrite provinces in the world (~ 15000 km^3) (de Silva et al., 2015). Most of these ignimbrites originated from collapse calderas that were active mainly from ca. 11–3 Ma, the exception being the ~ 1 Ma Purico caldera. The largest calderas in the APVC are La Pacana (2500 km^3; Lindsay et al., 2001), Vilama (1200 km^3; Soler et al., 2007), Kapina (1000 km^3; de Silva, 1989; Salisbury et al., 2011), Pastos Grandes (1500 km^3; Salisbury et al., 2011), Cerro Guacha caldera complex (2500 km^3; Grocke et al., 2017), Panizos (652 km^3; Ort, 1993) and Coranzulí (650 km^3; Seggiaro et al., 1987).

Previous studies on the Coranzulí caldera (Seggiaro et al., 1987, 2014a, 2014b, 2015; Seggiaro and Aniel, 1989; Seggiaro, 1994; Seggiaro and Hongn, 1994), permitted establishing the general stratigraphy, composition, and volume of its products, and the relation of the caldera to the local tectonic system, but the eruption dynamics and the mechanisms of caldera collapse remain poorly defined. According to these studies, the

Coranzulí caldera developed under strong structural controls due to its location at the intersection of several regional fault systems orientated N-S, NW-SE and NE-SW (Fig. 2). Like the other northeastern Puna calderas (Panizos; Ort, 1993; Vilama; Soler et al., 2007; Abra Granada volcanic complex; Caffe et al., 2008), it is dacitic-to-rhyodacitic and peraluminous in composition, and generated large volumes of crystal-rich ignimbrites.

The aim of this contribution is to establish the eruption dynamics and the mechanisms that led to the formation of the Coranzulí caldera. To achieve this objective, we reviewed the previous literature and conducted new field work, in order to constrain the stratigraphy, structural controls, and evolution of this caldera. We obtained a large number of new stratigraphic logs that, combined with previous information, offer a more detailed picture of the stratigraphic succession of the Coranzulí ignimbrite deposits. We also analyzed the contents and types of lithic fragments as a way of deciphering the source area of each ignimbritic flow unit. We also established a structural framework for the caldera and discuss how previous tectonic structures could have influenced its formation. Finally, we interpret the whole caldera-forming process in light of the evidence obtained.

2. Geological setting of the Coranzulí caldera

The Altiplano-Puna plateau is located to the east of an active volcanic arc and represents the internal part of the Andean orogen. It has an average elevation of 3,700 m a.s.l. and is characterized by an arid climate and endorheic drainage. The crust of the Puna is very thick, reaching up to 70 km in places (e.g. Beck et al., 2015). Although the deformation of the Puna and Eastern Cordillera started in the Paleogene (e.g. Hongn et al., 2007), the major uplift of the Puna did not take place until the Middle-Upper Miocene (e.g. Isacks, 1988; Allmendinger et al., 1986).

The present uplifted topography of the Puna has been interpreted as a result of tectonic shortening induced by the subducting Nazca plate and, to some extent, magmatic addition (Isacks, 1988; Allmendinger and Gubbels, 1996; Oncken et al., 2006). Between 22° and 24°S, the orogenic front of the Andes, located in the foreland fold and thrust belt of the Sub Andean Ranges, developed a thin-skin system (Aramayo Flores, 1989). On the other hand, the Eastern Cordillera and Puna have a thick-skin system, characterized by frequent reactivations of Paleozoic and Cretaceous faults. The regional detachment level has a smooth dip of ca. 6° from the orogenic front westwards, reaching an approximate depth of 20 km in the Puna region (Seggiaro and Hongn, 1999).

The Altiplano-Puna plateau is characterized by the presence of N-S, NW-SE and NE-SW trending lineaments, which define an area of sedimentation acting as highs that compartmentalize a series of basins (e.g. Salfity, 1985; Riller and Oncken, 2003; Riller et al., 2012). It has been recognized that the NW-SE major faults have, generally, oblique left-lateral slip components, whereas the NE-SW faults tend to have right-lateral movement (e.g. Riller and Oncken, 2003). Most volcanic centers in the Puna are situated within NW-SE trending lineaments. It is notable that the tectonic activity in the northern Puna and the Altiplano diminished considerably from ca. 8.8–7 Ma onwards (Cladouhos et al., 1994; Lamb and Hoke, 1997), as shown by the San Juan de Oro erosion surface (e.g. Gubbels et al., 1993). However, the Coranzulí and the Panizos ignimbrites erupted later (ca. 6–7 Ma) during a period in which records of deformation are scarce and are concentrated on the borders of the Altiplano (e.g. Sébrier et al., 1985).

The sedimentary basement at the Coranzulí area is formed by marine Ordovician deposits (pelites, sandstones, and quartzites), interlayered with a volcano-plutonic sequence (Coira, 1973). Although no outcrops of the pre-Ordovician basement are found in the northern Puna, the presence of accidental lithic fragments of sillimanitic gneiss

within the Coranzulí ignimbrites points to the existence of an unexposed basement beneath the Ordovician sediments (Seggiaro, 1994). The Cretaceous Pirgua Subgroup crops out in the Tanque Range (Fig. 2) and consists of red beds related to a rifting system; the contact between these rocks and the Ordovician beds is at a fault. Outcrops from the Cretaceous-Paleocene Balbuena Subgroup are only visible south of the Coyaguayma lineament. Paleogene fluvial successions and Neogene volcano-sedimentary successions can also be observed in the area (Alonso, 1986; Seggiaro and Aniel, 1989; Fig. 2).

3. Methods

In order to map the geology of the area including volcanic deposits and to establish its stratigraphy, facies correlations, and structural relations, we used Landsat 7 Enhanced Thematic Mapper (ETM) satellite images and earlier maps of the area (Seggiaro et al., 1987; Seggiaro, 1994; Coira et al., 2004; Seggiaro et al., 2014a; Seggiaro et al., 2015), and also conducted fieldwork. We established eleven new stratigraphic sections and describe their main vertical and lateral variations, as well as their thicknesses. These representative stratigraphic sections were compared to those previously established by Seggiaro et al. (1987) and used to complete a detailed description including all rock types and contacts, as well as petrographic and geochemical analyses that are beyond the scope of this contribution and will be presented elsewhere. All selected stratigraphic sections are shown in Figs. 3 and 4.

Stratigraphic descriptions include componentry analyses identifying the nature of the lithic fragments and their relative percentages. Lithic fragment types were discriminated in the field and verified through thin sections using a binocular microscope, while their relative percentages were estimated through visual comparison with percentage charts at every description point. Standard descriptions include color, degree

of induration and an account of textures and fabrics. The cartography of all the deposits was overlain on a geographical information system (GIS) platform (QGIS Geographic Information System: http://qgis.osgeo.org).

Previous structural data (e.g. Seggiaro et al., 1987; Seggiaro, 1994; Seggiaro and Hongn, 1994) including the attitude of the fault planes (strike and dip) and their sense of movement, were analyzed and complemented with new geologic mapping in order to help interpret the displacement of the major faults limiting the Coranzulí caldera.

4. Stratigraphy of Coranzulí caldera

The volcanic deposits at Coranzulí include a thick succession of syn-caldera ignimbrites emplaced inside and outside the caldera depression, along with a succession of 100-m-thick post-caldera dacitic lava flows emplaced inside the caldera (Figs. 2, 5). Some pre-caldera volcanic rocks now partially covered by syn-caldera ignimbrites are exposed in the north; they are block and ash-flow deposits formed by gravitational collapses of dacitic lava domes (see Las Cuevas stratigraphic section in Fig. 4).

The syn-caldera succession is composed entirely of ignimbrite deposits. No Plinian fallout deposits or any other type of volcanic tephra that may have immediately preceded the emplacement of these ignimbrites has been found. The Coranzulí ignimbritic succession unconformably covers Ordovician, Cretaceous, and/or Cenozoic deposits that form the volcano-sedimentary basement of this region (Fig. 2). According to previous studies (Seggiaro, 1994; Seggiaro et al., 1987; Seggiaro et al., 2014a) we also identified four major ignimbritic flow units emitted from the Coranzulí caldera. They all spread mainly north-, east-, south- and northwestwards from the caldera, reaching distances of up to 45 km from the vent. The contacts between the ignimbrite units are locally marked by sharp planar contacts, by the presence of a thin, crystal-rich, fines-depleted surge layer, between two ignimbrite depositional units, or by the presence of co-

ignimbrite lag breccias in proximal areas. In many other places the contacts are less well-defined and the ignimbrite successions even appear as a single unit, despite changing laterally into a deposit composed of several flow units (see stratigraphic sections of Quebrada Lulchaijo and Abra Grande in Fig. 3). All ignimbritic deposits are gray, crystal-rich, and poorly-to-densely welded (Fig. 6 a, b), with variable pumice content (5–30%, exceptionally 50 vol.%) and lithic fragment content (usually < 10 vol.%; exceptionally 25%). Pumices in all these ignimbrites have dacitic composition (see Seggiaro et al., 1987).

Subrounded-to-subangular lithic fragments of dacitic lavas are found throughout the ignimbritic succession but mostly in the basal unit. Ordovician metapelites and quartzites predominate in the second unit. The third and fourth units contain small amounts of sillimanitic gneiss derived from an unexposed basement, in addition to the same types as in the lower units. Lithic fragments of dacitic ignimbrites are only observed in the uppermost unit. Other lithic fragments present in the succession but in minor proportions include granitoids, porphyritic dacites and red pelites.

Juvenile fragments are very similar in all the Coranzulí ignimbrites and consist of variably vesicular, white-to-yellowish pumice (Fig. 6 a), which depending on the ignimbrite unit and their position in the vertical succession, may appear from subrounded-to-highly-welded fiamme, pink, gray or black in color (Fig. 6 b); the maximum observed size of juvenile fragments is 40 cm. A third type of juvenile fragment are fine-to-coarse-grained, dense, gray co-magmatic holocrystalline subrounded (crystal mush) clasts (Fig. 6 c). They are usually bigger and more abundant near caldera rims, reaching up to 3 vol.%. and up to 30 cm in size (exceptionally 70 cm). Both pumices and co-magmatic crystal-rich fragments (crystal mushes) have the same mineralogy and composition but a different degree of crystallinity.

The Coranzulí ignimbrites are dacitic (66–68 wt.% of SiO_2; Seggiaro et al., 1987) in composition and are crystal-rich, in terms of both their matrix (45–60 vol.%) and pumice (30–50 vol.%) content. The phenocrysts include plagioclases, biotites, quartz, minor sanidine, Fe-Ti oxides, apatite and zircon (Fig. 7 a, b).

The lack of erosional surfaces, sedimentary deposits, or paleosoils between the ignimbrite units suggest that each flow unit was emplaced by successive pulses during a single eruptive event. Some of the units overlap and cover most of the topographic depressions around the caldera, and form an ignimbritic plateau (Fig. 6 d). The maximum thicknesses of the individual deposits are in the range 40–130 m, with a maximum cumulative thickness of 380 m in an extra-caldera setting (stratigraphic section of Quebrada Lulchaijo; Fig. 3) where the base of the succession is exposed.

Seggiaro (1994) obtained three K-Ar ages of 6.8 ± 0.15, 6.6 ± 0.15, and 6.45 ± 0.15 Ma for the biotite crystals in the Coranzulí ignimbrites, with an average age of 6.6 ± 0.15 Ma representing the age of the eruption. Aquater (1979) obtained a K-Ar age of 6.73 ± 0.2 Ma in biotites for the rhyodacites to the south of Cerro Coranzulí in the post-caldera lavas, which suggests that the emplacement of these lavas occurred shortly after the formation of the caldera.

The lowermost ignimbrite unit unconformably covers pre-caldera volcanic deposits (block and ash-flow deposits) to the north of the caldera. It was emplaced north- and northwestwards from the caldera and has an average thickness of 50 m. At some locations, the caldera-related succession begins with a thin, 6-m-thick, laminated pyroclastic surge deposit that is succeeded transitionally by a 10-m-thick indurated, pyroclastic breccia with abundant pumice (60 vol.%), subangular lithic fragments of dacitic lava and minor Ordovician metapelites within a fine ash matrix (see Las Cuevas stratigraphic section in Fig. 4). In agreement with Seggiaro et al (1987), we interpret this

breccia as a co-ignimbrite lag breccia found only on the north flank of Coranzulí volcano, where it is partially covered by the second and third ignimbrite units. In medial facies to the NW of Cerro Coranzulí, the first ignimbrite is characterized by the presence of lithic fragments (5 vol.%) of dacitic lava, similar to those present in the proximal basal breccia, together with minor contents of Ordovician metapelites and quartzites. It is rich in quartz, plagioclase and biotite crystals (~ 40 vol.%) and moderately welded. Pumice is variable in size, reaching up to 25 cm in diameter, and generally appears slightly deformed in proximal facies, although towards the top the unit is more welded exhibiting columnar jointing and elongated fiamme.

The second ignimbrite unit was dispersed in all directions (see Fig. 5) and its thickness ranges from 60 to 130 m. The contact with the first unit is observed in the Quebrada Lulchaijo stratigraphic section (Fig. 3), where a 2-cm-thick crystal-rich ash layer followed by a 15-cm-thick crystal-rich pyroclastic surge deposit of stratified lapilli with parallel and cross stratification are visible. This deposit is interpreted as formed from an ash-cloud surge accompanying the emplacement of the first ignimbrite flow unit. However, in proximal facies (Las Cuevas stratigraphic section; Fig. 4) this contact is marked by a co-ignimbrite breccia formed of large blocks of dacitic lava and smaller—but more abundant—lithic clasts of Ordovician metapelite immersed in a pyroclastic matrix. Locally this massive ignimbrite is densely-welded and crystal-rich (35–40 vol.%) and has some layers with concentrations of pumices, probably related to local changes in topography (e.g. Pittari et al., 2005). In some zones its texture is eutaxitic and it is defined by parallel, intensely flattened fiamme.

The third ignimbrite unit was emplaced east-, north- and northwestwards for short distances but mainly southwards over distances of up to 45 km, with an average thickness of 40 m. The contact with the second unit is marked by a 6-m-thick co-ignimbrite lag

breccia found in the Casa Blanca stratigraphic profile (see Fig. 4), and by a lithified ash layer at Lulchaijo (see Fig 3). The breccia consists of large blocks, up to 80 cm in length, which consist of Ordovician metapelites, dacitic lavas, minor gneiss and abundant co-magmatic dense lithic fragments (Fig. 6 c), and smaller lithic fragments of around 5 cm of the same nature. The ignimbrite is massive and crystal-rich (above 40 vol.%) with variable degrees of welding, increasing towards the top and with distance. In some sections there are levels rich in pumices (Baños Termales stratigraphic section; Fig. 4) and lenticular layers concentrated in lithic fragments (Norte de Coranzulí stratigraphic section; Fig. 4). Pumice is rich in phenocrysts and appears stretched parallel to the flow direction, mainly concentrated towards the upper part of the ignimbrite unit, where the ignimbrite is usually welded showing abundant fiamme and columnar jointing (Fig. 6 e). This unit contains lithic fragments of various types including two types of dacite, one porphyritic and other aphanitic; metapelites and quartzites from the Ordovician basement; a few sillimanitic gneiss; and red pelites and sandstones. In comparison with the previous units, this unit is poorer in lithics, although its bulk content of pumice fragments is greater than that of the other pyroclastic units.

The fourth ignimbrite unit was emplaced only to the south. In proximal settings (Section 11 in Fig. 4) the succession outcrops, albeit without an exposed base. In its lower part a co-ignimbritic lag breccia occurs, containing blocks of up to 50 cm in length of a dacitic ignimbrite, and lithics of Ordovician metapelite, dacitic lava, and metamorphic basement fragments. The breccia grades into alternating stratified and massive layers of pumice-rich (ca. 15–30 vol.%) ignimbrite, up to 70 m in thickness, which is rich in dense co-magmatic fragments that reach 30 cm in diameter. It is densely welded and exhibits well-developed columnar jointing.

The intra-caldera ignimbritic succession was uplifted several hundred metres by a resurgent dome (Fig. 6 f), which is poorly exposed and affected by strong hydrothermal alteration (Fig. 6 g), thereby hampering the recognition of original lithological features.

Post-caldera volcanism erupted dacitic lavas that cover the intra-caldera ignimbrites at Cerro Coranzulí (Figs. 2 and 6 g). In all, there are three lava flows in the central area of the caldera that are massive-to-banded and occasionally brecciated. These lavas have a short run-out and reach thicknesses of up to 100 m. They are porphyritic or seriate, and contain phenocrysts of plagioclase, amphibole, quartz, pyroxene and minor biotite, K-feldspar and Fe-Ti oxides.

5. Coranzulí tectonic framework

From Neogene times onwards, the trend of convergence between the Nazca and South American plates has been N75°E (Pardo-Casas and Molnar, 1987), but the principal horizontal shortening direction is E-W (Isacks, 1988; Allmendinger et al., 1997; Kley and Monaldi, 1998). The Altiplano-Puna is characterized by the presence of N-S, NW-SE and NE-SW regional faults (e.g. Salfity, 1985; Riller and Oncken, 2003), the first ones being orogen-parallel sinistral thrust faults that have driven Paleozoic rocks over Cenozoic ones (e.g. Allmendinger et al., 1997; Riller and Oncken, 2003). The other faults are either dextral, reverse faults (in the case of the NE-SW trending faults) or strike-slip faults formed mainly under an overall left-lateral transtension (NW-SE trending faults) (e.g. Allmendinger et al., 1983; Acocella et al., 2011; Riller et al., 2012). The interaction of these three fault systems defines rhomboid-shaped deformation domains— internally drained basins—in the upper crust that are a result of its segmentation by shortening (Riller and Oncken, 2003) and defines transpressive deformation (e.g. Coutand et al., 2001). In the northern Puna, due to the above-mentioned crustal shortening gradient (Riller et al., 2012), the rhomboid-shaped basins are smaller but are also more abundant than in southern Puna.

The Coranzulí complex is emplaced at the convergence of faults with N-S, NE-SW and NW-SE strikes (Figs. 2 and 5). Seggiaro and Hongn (1994) recognized that all of these faults were active before the formation of the caldera and were then reactivated during the caldera eruption. However, their sense of movement was interpreted only based on some striae data (Seggiaro, 1994; Seggiaro and Hongn, 1994). Our new field observations allowed revision of the structural framework of the Cerro Coranzulí, giving more weight to the main displacements observed by the major faults that uplifted ranges and the ones that produced subhorizontal displacements. The geological mapping of the area (Fig. 2) allows us to interpret the main movements by taking into account the relative ages of the affected units. The approximately N-S faults are responsible for main thrusts with opposite vergences, whereas the transversal faults generally behave by means of lateral transference zones that compensate those differential thrusts displacements. These lateral structures are in many cases induced by basement anisotropies due to old faults or from sudden lithologic changes (e.g. Hongn et al., 2010). North and South of the Coranzulí caldera, two ranges were uplifted by thrusts with opposite main vergences leading to the formation of a NW-SE transference zone. North of the Coranzulí caldera, the Carahuasi Range is oriented approximately N-S, (see Fig. 2) and resulted from the uplift of Ordovician sedimentary deposits over a Miocene volcano-sedimentary succession by a thrust with west vergence (Fig. 2). South of the Coranzulí caldera, the Tanque Range (Fig. 2) is affected by a set of overthrusts, involving several units (Ordovician granitoids, Salta Group sedimentary sequences and Neogene volcano sedimentary successions) with opposite vergences, of which the most significant has eastward vergence (Fig. 2). The lithologic changes between the Carahuasi and Tanque ranges (Fig. 2) and their opposite vergences may indicate that they had behaved as a structural weakness zone that favored the differential displacement of about 10 km between them, thus leading to the transversal NW-SE belt of the Coyaguayma lineament, including the Coyaguayma and Ramallo faults with sinistral kinematics (Figs. 2, 5). Hence, based on a detailed geologic map of the area, the sense of displacement of these faults is reinterpreted from the formerly dextral movement interpreted by Seggiaro and

Hongn (1994) based on striae data of secondary faults measured in Miocene volcano-sedimentary sequences.

The Ramallo and Coyaguayma faults delimited a Miocene volcano-sedimentary basin, formed previous to the eruption of the Coranzulí caldera. Other important tectonic activity in the area just before the Coranzulí eruption is recorded in the area affected by the Tanque fault system, where Coranzulí ignimbrites lay in angular unconformity above deformed Neogene volcano-sedimentary successions dated at 6.9 Ma (Alonso, 1986), thus delimiting a tectonic activity interval prior to the Coranzulí eruption— between 6.9 and 6.8 Ma (Trumbull et al., 2006). The continuation of the Tanque thrust system to the north of Cerro Coranzulí adopts a NE-SW strike represented by the Doncellas Fault of dextral transcurrent kinematics (Seggiaro, 1994; Seggiaro and Hongn, 1994).

The Coranzulí complex is thus emplaced at the convergence of several regional fault systems: the Coyaguayma and Ramallo NW-SE sinistral strike-slip faults, the Doncellas NE-SW dextral strike-slip fault, and the Tanque and Carahuasi N-S thrust faults with opposite vergences (Figs. 2 and 5). All of these faults were active before the formation of the caldera and were then reactivated during the caldera eruption (Seggiaro and Hongn, 1994). Indeed, the caldera boundaries coincide in part with the Coyaguayma fault (southern border), the Ramallo fault (northwestern border), the intersection of the Ramallo and Doncellas faults (northern border) and the Tanque fault in addition to all of their associated secondary faults (western border) (Fig. 5), which is evidence of how these pre-existing fault systems helped define the Coranzulí caldera ring-fault. In Figure 5 we show the orientation and sense of movement of the main faults in the Coranzulí caldera, in which the extensional axis runs approximately, NNE-SSW relative to the convergence of the Doncellas, Ramallo, Coyaguayma, Tanque and Carahuasi faults and their senses of displacement.

6. Discussion

We postulate that the intersection and relative movement of regional faults such as the ones described above played a fundamental role during the Upper Miocene in the accumulation of a large volume of silicic magma in the upper crust below the Coranzulí volcanic complex. Moreover, the convergence of the Carahuasi, Tanque, Doncellas, Ramallo, and Coyaguayma faults and their relative senses of displacement, allowed defining an extensional axis running in a NNE-SSW direction in the Coranzulí area (see Fig. 5) that was paramount to the formation of the caldera.

The Coranzulí caldera-forming eruption generated four main ignimbritic pulses that emplaced the four principal ignimbrite units in different directions from the caldera. The lack of any erosional surfaces, sedimentary deposits, or paleosoils separating the ignimbrite units suggests that they were emplaced almost uninterrupted in time, probably in a nearly continuous mass supply from the caldera.

The absence of any Plinian fallout deposits at the base of the ignimbrite succession highlights the fact that the pyroclastic currents formed as soon as the eruption began, as previously suggested by Seggiaro et al. (1987). Therefore, the caldera collapse occurred at the beginning of the eruption, without any previous significant decompression of the magma chamber (see Martí et al., 2009; Costa and Martí, 2016), which suggests a possible tectonic trigger and strong tectonic influence in the formation and control of the ring faults (see Costa and Martí, 2016). In fact, the local extensional stress field found at the site of the Coranzulí complex would have favored ascent and accumulation of silicic magma below the current Coranzulí caldera, the subsequent conduit opening and extrusion of the pyroclastic material and the formation of the caldera.

Moreover, the relatively minor depletion of fines (i.e. relatively similar crystal content of pumices and matrix in each ignimbrite unit) through elutriation in the

Coranzulí ignimbrites indicates that the flows that fed the pyroclastic currents were concentrated and not much thicker than the resulting deposits. The high degree of welding of some deposits, both in proximal and distal facies, also supports this interpretation as it indicates thermal conservation within the flow. If deposits are to travel long distances and maintain these characteristics, the flows must have been fed by long-lasting eruptive pulses that produced very low eruptive columns that collapsed almost immediately, i.e. boiling-over eruptions (e.g. Soler et al., 2007; Guzmán and Petrinovic, 2010; Pacheco-Hoyos et al., 2018) providing a high mass flow rate (e.g. Cas et al., 2011; Costa and Martí, 2016).

Co-ignimbrite lag breccias are common in many ignimbrites derived from collapse calderas and they are mostly interpreted as representing the vent opening phases (Druitt and Sparks, 1982; Walker, 1985; Druitt, 1985; Druitt and Bacon, 1986; Suzuki-Kamata et al., 1993; Rosi et al., 1996; Pittari et al., 2008; Petrinovic et al., 2010). These breccias contain fragments from the rocks that form the stratigraphic succession above the magma chamber. The presence of co-magmatic crystal-rich ("crystal mush") fragments in these breccias is the evidence that fragmentation was reaching the magma chamber (see Fulignati et al., 2004; Costa and Martí, 2016), so in the case of the Coranzulí caldera we interpret this as evidence for the initiation of caldera collapse. The fact that the co-ignimbrite lag breccias contain accidental lithic fragments of a different nature in the different ignimbrites is considered to be evidence for the opening of the ring fault at different times depending on the affected sector of the caldera (e.g. Suzuki-Kamata et al., 1993; Pittari et al., 2008), which implies that the caldera collapse process was not always homogeneous (i.e. it did not occur in a purely piston-like fashion).

The irregular distribution (i.e. non-radial) of some of the ignimbrites and the distribution and composition of their associated co-ignimbrite lag breccias help to infer

the location of the vents (i.e. which sector of the caldera rims), suggesting that caldera collapse occurred with different ring fault sectors operating at different times. This implies that caldera collapse evolved sequentially throughout the whole ring fault, favored by the combined effect of the above mentioned Ramallo, Coyaguayma, Carahuasi, Tanque and Doncellas fault systems. The existence of erosion or coverage by newer deposits hinders the recognition of ring fractures in some sectors of the Coranzulí caldera. While the western border does show vertical faults accommodating the collapse (see Fig. 6 h), the eastern border is the least evident, having been partially eroded and covered by new deposits.

However, as discussed before, the location of co-ignimbritic lag breccias was very important for the identification of the caldera rims. On its northern border the presence of the co-ignimbritic lag breccias associated with the lowermost ignimbrite unit indicates that this caldera border opened early in the eruption and was driven by the Doncellas and Ramallo faults, which acted as the main structural control during these first stages of the Coranzulí caldera collapse. The distribution of the first ignimbrite being only north-to-northwestwards also suggests 'trapdoor' behavior during the first pulse of the caldera collapse (Fig. 8 a). Conversely, the second ignimbrite flow unit was emplaced radially around the Coranzulí volcanic complex, thereby indicating the presence of an eruption throughout the whole (or, most of) the caldera ring-fault, and more continuous subsidence of the caldera block (i.e. piston-like) (Fig. 8 b). The third ignimbrite flow unit, also associated with a prominent co-ignimbrite lag breccia, was largely emplaced radially, albeit with very limited eastward flows (Fig. 8 c). In this succession, there are some metamorphic lithic fragments, which may indicate a deeper level of fragmentation in this third caldera collapse pulse as these rocks do not crop out in the surroundings. Finally, the fourth ignimbrite is associated with a co-ignimbrite lag breccia containing lithic clast

fragments of ignimbrites in addition to the same lithic fragments observed in the lower ignimbrite units. This indicates a widening of the caldera rim and a change in the collapse dynamics, this time behaving again as a 'trapdoor' (Fig. 8 d), as this flow unit is only observed to be oriented in a southward direction. The fact that this last ignimbrite is so restricted in its present occurrence may be either an erosional feature or because the volume of compressible magma remaining (i.e. it is able to expand and fragment) was much less in this last pulse, or both. The inferred structural rim of the caldera is thus 16 x 12 km, elongated in a N-S to NNE-SSW direction, and reflects the potential influence of local and regional tectonics in its formation and definition.

Cerro Coranzulí is a resurgence dome in the central part of the caldera where hundreds of meters of intensely altered intracaldera ignimbrites are exposed (see Fig. 6 g), visible from satellite images. The top of Cerro Coranzulí is covered by post-caldera lavas (Figs. 2; 6 g; 8 e).

The interpreted evolution for the collapse of Coranzulí caldera is also confirmed by the distribution of lithic fragments throughout the Coranzulí ignimbrite succession. As noted by Seggiaro et al. (1987) and Seggiaro (1994), the dominant lithic composition varies throughout the whole ignimbritic succession and differs according to the flow directions. This may be explained by the diverse composition of the caldera substrate (e.g. Suzuki-Kamata et al., 1993; Pittari et al., 2008) and/or by varying disruption levels during caldera collapse (Seggiaro, 1994). In this sense, the sequential opening of the ring fault described above suggests that the first caldera collapse pulse was localized at the northern and western rims. This is suggested by the fact that the main lithics at the base of the first ignimbrite unit are dacitic lavas but also include Ordovician metapelites throughout most of the remaining pyroclastic sequence. There is no solid evidence to help us interpret when and how the collapse proceeded along the eastern rim, although the radial

distribution of the second ignimbrite unit suggests that the eastern margin was probably already opened at that time. The southern margin was probably the last to be activated or, rather was where the final activity representing caldera widening was concentrated.

Despite there being no direct evidence, we speculate that the fact that the Coranzulí caldera behaved as a trapdoor collapse, and then collapsing along all of the ring faults, before switching back again to trapdoor collapse, is due to the control that the local tectonic structure and the different strengths of basement rocks located at different sectors of the Coranzulí complex, affected how the magma chamber opened to the surface and on how the ring fault system progressed during caldera collapse. The central Andes offers a wide range of collapse calderas developed under the influence of local and regional tectonics (e.g. de Silva, 1989; Petrinovic et al., 2010; Folkes et al., 2011), but the exact interplay between volcanism and tectonics during caldera formation is still not well understood in most of them. The Coranzulí caldera is just a particular example showing this combination of trapdoor to full-on collapse, but it may not be the only one that shows evidence of a heterogeneous collapse event, as seems to have also occurred in the Panizos caldera (Ort, 1993). Fault opening depends on the configuration of tectonic stresses around the fault plane and on the strength of the rock along it (see Gudmundsson, 2011, 2013; Boneh and Reches, 2018). In the case of caldera faults in which part of them may be lubricated by the presence of overpressurized magma, the situation may be even more complex, as the slip along lubricated and non-lubricated fault planes may be totally different, thus affecting the rate and style of collapse (Spray, 1997; Kokelaar, 2007). These anisotropies along the ring fault systems may be difficult to test through experimental or numerical models, currently being widely used to understand and explain caldera collapse dynamics (see Martí et al., 2008; Geyer and Martí, 2014, for recent reviews on caldera modeling), but may be inferred and approached through the inspection

of natural examples, such as the one presented herein. With this, we point towards the importance of knowing more about tectonic influence and fault behavior in order to understand caldera dynamics, in particular for those of large dimensions.

7. Conclusions

The Coranzulí caldera (23°00'S-66°15'W) is the easternmost caldera of the northern Puna and is probably one of the least known in the whole region, despite it presenting interesting clues to understand caldera collapse processes.

The formation of the Coranzulí caldera was structurally controlled and did not require any significant pre-caldera decompression in the magma chamber. The intersection of several faults where the caldera is located was the main factor causing conduit opening, ascent and extrusion of the pyroclastic material and caldera collapse. These faults display N-S, NW-SE, and NE-SW trends and an extensional axis with a NNE-SSW trend, coinciding with the elongation of the 16 x 12 km caldera. The ignimbritic flows were fed by a boiling-over type eruption that generated a very low eruptive column with high mass flow rates but with no Plinian fallout deposits.

Four different ignimbrite flow units are recognized, each representing different successive pulses within a single eruption. The irregular distribution shown by some of the Coranzulí ignimbrites and the emplacement of co-ignimbrite lag breccias record the position of the caldera ring-faults. At the beginning of the eruption the ring fault opened north- and northwestwards in a 'trapdoor' fashion, thereby generating the first ignimbrite flow unit. Immediately afterwards, the whole ring fault opened during the eruption of the second flow unit and continued to do so during the eruption of the third flow unit. The final stage of the caldera evolution involved a widening of the ring fault and a change in

the collapse style towards a 'trapdoor' caldera that emitted the fourth ignimbrite flow unit southwards.

The dominant composition of the lithic fragments within the ignimbrites varies stratigraphically, with dacitic lava fragments predominating the first ignimbrite unit, Ordovician metapelites, and quartzites that are mostly concentrated in the second and third ignimbrites; with sillimanitic gneiss appearing only in the third and fourth ignimbrite units, this last one also contains dacitic ignimbrite lithic fragments. Sillimanitic gneiss is not exposed elsewhere in the area, and so its appearance indicates that the final stages of the collapse reached deeper levels.

Acknowledgments

SG would like to thank the Progama de Financiamiento Parcial para Investigadores run by CONICET that facilitated a research period of two years at the Instituto de Ciencias de la Tierra Jaume Almera (CSIC). SG is also grateful to Agencia Nacional de Promoción Científica y Técnica (PICT 419-2012) and the Consejo Nacional de Investigaciones Científicas y Técnicas (PUE 2016-2021) Argentina, and also to Elena López, Albano Floridia, and Emanuel Ramos for their assistance in the field and Valmir da Silva Souza for helpful discussions. JM was supported by grant CGL2017-84901-C2-1-P. The English text was reviewed and revised by Grant Buffett. We warmly thank the editor James Gardner and an anonymous referee for their constructive comments.

References

Acocella, V., Gioncada, A., Omarini, R., Riller, U., Mazzuoli, R., Vezzoli, L., 2011. Tectonomagmatic characteristics of the back-arc portion of the Calama–Olacapato–El Toro fault zone, Central Andes. Tectonics 30, TC3005.

Allmendinger, R., 1986. Tectonic development, southeastern border of the Puna plateau, northwestern Argentina Andes. Geol. Soc. Am. Bull. 97, 1070–1082.

Allmendinger, R., Gubbels, T., 1996. Pure and simple shear plateau uplift, Altiplano–Puna, Argentina and Bolivia. Tectonophys. 259, 1–13.

Allmendinger, R.W., Ramos, V.A., Jordan, T.E., Palma, M., Isacks, B.L., 1983. Paleogeography and Andean structural geometry, northwest Argentina. Tectonics 2 (1), 1–16.

Allmendinger, R.W., Jordan, T.E., Kay, S.M., Isacks, B.L., 1997. The evolution of the Altiplano–Puna Plateau of The Central Andes. Ann. Rev. Earth Planet. Sci. 25, 139–174. https://doi.org/10.1146/annurev.earth.25.1.139

Alonso, R. N., 1986. Ocurrencia, posición estratigráfica y génesis de los depósitos de boratos de la Puna Argentina. Ph.D. Thesis, Universidad Nacional de Salta, Argentina.

AQUATER S.A., 1979. Estudio del potencial geotérmico de la provincia de Jujuy, República Argentina. Secretaría de Minería de la Provincia de Jujuy, Argentina.

Aramayo Flores, F., 1989. El cinturón plegado y sobrecorrido del norte argentino. Boletín de Informaciones Petroleras, Tercera Época 17, 2–16.

Beck, S., Zandt, G., Ward, K., Scire, A., 2015. Multiple styles and scales of lithospheric foundering beneath the Puna Plateau, central Andes. In: DeCelles, P.G., Ducea, M.N., Carrapa, B., Kapp, P.A. (Eds.), Geodynamics of a Cordilleran Orogenic System: The Central Andes of Argentina and Northern Chile. Geol. Soc. Am. Memoirs 212, pp. 43–60.

Boneh, Y., Reches, Z., 2018. Geotribology - Friction, wear, and lubrication of faults Tectonophys. 733, 171–181.

Caffe, P.J., Soler, M.M., Coira, B.L., Onoe, A.T., Cordani, U.G., 2008. The Granada ignimbrite: a compound pyroclastic unit and its relationship with Upper Miocene caldera volcanism in the northern Puna. J. South Am. Earth Sci. 25, 464–484.

Cas, R. A. F., Wright, H. M. N., Folkes, C. B., Lesti, C., Porreca, M., Giordano, G., Viramonte, J. G., 2011. The flow dynamics of an extremely large volume pyroclastic flow, the 2.08-Ma Cerro Galán Ignimbrite, NW Argentina, and comparison with other flow types. Bull. Volcanol. 73 (10), 1583–1609. DOI 10.1007/s00445-011-0564-y

Cladouhos, T., Allmendinger, R., Coira, B., Farrar, E., 1994. Late cenozoic deformation in the Central Andes: fault kinematics from the northern Puna, northwestern Argentina and southwestern Bolivia. J. South Am. Earth Sci. 7 (2), 209–228.

Coira, B., 1973. Resultados preliminares sobre la petrología del ciclo eruptivo ordovícico concomitante con la sedimentación de la Formación Acoite en la zona de Abra Pampa, Provincia de Jujuy, Argentina. Rev. Asoc. Geol. Arg. 28 (1), 85–90.

Coira, B., Caffe, P.J., Ramírez, A., Chayle, W., Díaz, A., Rosas, S.A., Pérez, A., Pérez, E.M.B., Orosco, O., Martínez, M., 2004. Hoja Geológica 2366-I Mina Pirquitas 1:250.000. Instituto de Geología y Recursos Minerales, Servicio Geológico Minero Argentino, Boletín 269, Buenos Aires.

Costa , A., Martí, J., 2016. Stress field controls in high intensity explosive eruptions. Front. Earth Sci. 4, 92. doi: 10.3389/feart.2016.00092

Coutand, I., Cobbold, P., de Urreiztieta, M., Gautier, P., Chauvin, A., Gapais, D., Rossello, E., López Gamundi, O., 2001. Style and history of Andean deformation. Puna plateau, northwestern Argentina. Tectonics 20 (2), 210–234.

de Silva, S.L., 1989. Altiplano–Puna Volcanic Complex of the Central Andes. Geology 17, 1102–1106. https://doi.org/10.1130/0091-7613(1989)017<1102:APVCOT>2.3.CO;2

de Silva, S.L., Riggs, N.R., Barth, A.P., 2015. Quickening the pulse: Fractal tempos in continental arc magmatism. Elements 11(2), 113–118. https://doi.org/10.2113/gselements.11.2.113

Druitt, T.H., 1985. Vent evolution and lag breccia formation during the Cape Riva eruption of Santorini, Greece. J. Geol. 93, 439–454.

Druitt, T.H., Sparks, R.S.J., 1982. A proximal ignimbrite breccia facies on Santorini, Greece. J. Volcanol. Geotherm. Res. 13, 147–171.

Druitt, T.H., Bacon, C.R., 1986. Lithic breccia and ignimbrite erupted during the collapse of Crater Lake caldera, Oregon. J. Volcanol. Geotherm. Res. 29, 1–32.

Folkes, C.B., Wright, H.M., Cas, R.A.F., de Silva, S.L., Lesti, C., Viramonte, J.G., 2011. A re-appraisal of the stratigraphy and volcanology of the Cerro Galán volcanic system, NW Argentina. In: Cas RAF, Cashman K (Eds) The Cerro Galan Ignimbrite and Caldera: characteristics and origins of a very large volume ignimbrite and its magma system. Bull Volcanol. 73 (10):1427–1454. doi:10.1007/s00445-011-0459-y

Fulignati, P., Marinelli, P., Proto, M., Sbrana, S., 2004. Evidences for disruption of a crystallizing front in a magma chamber during caldera collapse: an example from the Breccia Museo unit (Campanian Ignimbrite eruption, Italy). J. Volcanol. Geotherm. Res. 133, 141–155.

Geyer, A., Martí, J., 2014. A short review of our current understanding of the development of ring faults during collapse caldera formation. Front. Earth Sci. 2: 22, doi:10.3389/feart.2014.00022

Grocke, S. B., de Silva, S. L., Wallace, P. J., Cottrell, E., Schmitt, A. K., 2017. Catastrophic Caldera-Forming (CCF) Monotonous Silicic Magma Reservoirs: Constraints from Volatiles in Melt Inclusions from the 3.49 Ma Tara Supereruption, Guacha II Caldera, SW Bolivia. J. Petrol. 58 (2), 227–260. https://doi.org/10.1093/petrology/egx012

Gubbels, T., Isacks, B., Farrar, E., 1993. High-level surfaces, plateau uplift, and foreland development, Bolivian central Andes. Geology 21, 695–698.

Gudmundsson, A., 2011. Rock Fractures in Geological Processes. Cambridge University Press. doi: 10.1017/CBO9780511975684

Gudmundsson, A., 2013. Great challenges in structural geology and tectonics. Front. Earth Sci. doi: 10.3389/feart.2013.00002

Guzmán, S., Petrinovic, I., 2010. The Luingo caldera: the south-easternmost collapse caldera in the Altiplano–Puna plateau, NW Argentina. J. Volcanol. Geotherm. Res. 194, 174–188.https://doi.org/10.1016/j.jvolgeores.2010.05.009

Guzmán, S., Grosse, P., Martí, J., Petrinovic, I.A., Seggiaro, R., 2017. Calderas cenozoicas argentinas de la Zona Volcánica Central de los Andes – procesos eruptivos y dinámica: una revisión. In: Muruaga, C.M., Grosse, P. (Eds.), Ciencias de la Tierra y Recursos Naturales del NOA. Relatorio del XX Congreso Geológico Argentino, San Miguel de Tucumán, Argentina, pp. 518–547.

Hongn, F., del Papa, C., Powell, J., Petrinovic, I., Mon, R., Deraco, V., 2007. Middle Eocene deformation and sedimentation in the Puna–Eastern Cordillera transition (23°–26° S): control by preexisting heterogeneities on the pattern of initial Andean shortening. Geology 35 (3), 271–274.

Hongn, F., Mon, R., Petrinovic, I., del Papa, C., Powell, J., 2010. Inversión y reactivación tectónicas cretácico cenozoicas en el Noroeste Argentino: influencia de las heterogeneidades del basamento neoproterozoico-paleozoico inferior. Rev. Asoc. Geol. Arg. 66 (1-2), 38–53.

Isacks, B., 1988. Uplift of the Central Andean Plateau and bending of the Bolivian Orocline. J. Geophys. Res. 93 (4), 3211–3231. https://doi.org/10.1136/hrt.59.4.429

Kley, J., Monaldi, C.R., 1998. Tectonic shortening and crustal thickness in the Central Andes: how good is the correlation?. Geology 26, 723–726.

Kokelaar P., 2007. Friction melting, catastrophic dilation and breccia formation along caldera superfaults. J. Geol. Soc. London 164(4), 751–754.

Lamb, S., Hoke, L. 1997. Origin of the high plateau in the Central Andes, Bolivia, South America. Tectonics 16, 623–649. https://doi.org/10.1029/97TC00495

Lindsay, J.M., de Silva, S., Trumbull, R., Emmermann, R., Wemmer, K., 2001. La Pacana caldera, N. Chile: a re-evaluation of the stratigraphy and volcanology of one of the world's largest resurgent caldera. J. Volcanol. Geotherm. Res. 106, 145–173. https://doi.org/10.1016/S0377-0273(00)00270-5

Martí, J., Geyer, A., Folch, A., Gottmann, J., 2008. A review on collapse caldera modelling. In: Gottmann, J., Martí, J. (Eds.), Caldera Volcanism: Analysis, Modelling and Response. Developments in Volcanology. Elsevier, Amsterdam, pp. 233–284.

Martí, J., Geyer, A., Folch, A., 2009. A genetic classification of collapse calderas based on field studies, and analogue and theoretical modelling. In: Thordarson, T., Self, S., Larsen, G., Rowland, S.K., Hoskuldsson, A. (Eds.), Studies in Volcanology: The Legacy of George Walker. Special Publications of IAVCEI, 2. Geological Society, London, pp. 249–266.

Oncken, O., Hindle, D., Kley, J., Elger, K., Victor, P., Schemmann, K., 2006. Deformation of the Central Andean Upper Plate System-Facts, Fiction, and constraints for plateau models. In: Oncken, O., Chong, G., Franz, G., Giese, P., Götze, H., Ramos, V., Strecker, M., Wigger, P. (Eds.), The Andes - Active Subduction Orogeny, Springer-Verlag, Berlin, pp. 265–283.

Ort, M., 1993. Eruptive processes and caldera formation in a nested downsag collapse caldera: Cerro Panizos, central Andes Mountains. J. Volcanol. Geotherm. Res. 56, 221–252. https://doi.org/10.1016/0377-0273(93)90018-M

Pacheco-Hoyos, J.G., Aguirre-Díaz, G.J., Dávila-Harris, P., 2018. Boiling-over dense pyroclastic density currents during the formation of the ~ 100 km^3 Huichapan ignimbrite in Central Mexico: Stratigraphic and lithofacies analysis. J Volcanol. Geotherm. Res. 349, 268–282. https://doi.org/10.1016/j.jvolgeores.2017.11.007

Pardo-Casas, F., Molnar, P., 1987. Relative motion of Nazca (Farallón) and South American plates since Late Cretaceous time. Tectonics 6, 233–248. https://doi.org/10.1029/TC006i003p00233

Petrinovic, I.A., Martí, J., Aguirre-Díaz, G.J., Guzmán, S.R., Geyer, A., Salado Paz, N., 2010. The Cerro Aguas Calientes caldera, NW Argentina: an example of a tectonically controlled polygenetic collapse caldera, and its regional significance. J. Volcanol. Geotherm. Res. 194, 15–26. https://doi.org/10.1016/j.jvolgeores.2010.04.012

Pittari, A., Cas, R.A.F., Martí, J., 2005. The occurrence and origin of prominent massive, pumice-rich ignimbrite lobes within the Late Pleistocene Abrigo Ignimbrite, Tenerife, Canary Islands. J. Volcanol. Geotherm. Res. 139, 271– 293.

Pittari, A., Cas, R.A.F., Wolff, J.A., Nichols, H.J., Larson, P.B., Martí, J., 2008. Chapter 3 The Use of Lithic Clast Distributions in Pyroclastic Deposits to Understand Pre- and Syn-Caldera Collapse Processes: A Case Study of the Abrigo Ignimbrite, Tenerife, Canary Islands. Dev. Volcanol. https://doi.org/10.1016/S1871-644X(07)00003-4

Riller, U., Oncken,O., 2003.Growth of the central Andean plateau by tectonic segmentation is controlled by the gradient in crustal shortening. J. Geology 111, 367–384.

Riller, U., Cruden, A. R., Boutelier, D., Schrank, C. E., 2012. The causes of sinuous crustal-scale deformation patterns in hot orogens: Evidence from scaled analogue experiments and the southern Central Andes. J. Struct. Geology 37, 65–74.

Rosi, M., Vezzoli, L., Aleotti, P., De Censi, M., 1996. Interaction between caldera collapse and eruptive dynamics during the Campanian Ignimbrite eruption, Phlegraean Fields, Italy. Bull. Volcanol. 57, 541–554.

Salisbury, M.J., Jicha, B.R., de Silva, S.L., Singer, B.S., Jiménez, N.C., Ort, M.H., 2011. $^{40}Ar/^{39}Ar$ chronostratigraphy of Altiplano-Puna volcanic complex ignimbrites reveals the development of a majormagmatic province. Geol. Soc. Am. Bull. 123 (5–6), 821–840. https://doi.org/10.1130/B30280.1

Salfity, J.A., 1985. Lineamientos transversales al rumbo Andino en el noroeste Argentino. IV Congreso Geologico Chileno, Antofagasta, Chile, 2, pp. 119–137.

Sébrier, M., Mercier, J. L., Mégard, F., Laubacher, G., Carey-Gailhardis, E., 1985. Quaternary normal and reverse faulting and the state of stress in the Central Andes of south Perú. Tectonics, 4 (7), 739–780.

Seggiaro, R.E., 1994. Petrología, geoquímica y mecanismos de erupción del complejo volcánico Coranzulí. Ph.D. Thesis, Universidad Nacional de Salta, Argentina.

Seggiaro, R., Aniel, B., 1989. Los ciclos piroclásticos cenozoicos del área Tiomayo Coranzulí Jujuy Argentina. Rev. Asoc. Geol. Arg. 44, 394–401.

Seggiaro, R., Hongn, F., 1994. Tectónica transcurrente asociada al volcán Coranzulí, Jujuy, Argentina. 7º Congreso Geológico Chileno, Concepción, Chile, 1, pp. 169–173.

Seggiaro, R., Hongn, F., 1999. Evolución orogénica y volcanismo cenozoico en el noroeste de Argentina. In: Colombo, F., Querault, I., Petrinovic, I. (Eds.), Geología de los Andes Centrales Meridionales: El Noroeste Argentino. Acta Geológica Hispánica 34, pp. 227–242.

Seggiaro, R.E., Gorustovich, S. A., Martí, J., 1987. Las ignimbritas del Complejo Volcánico Coranzulí (Puna Argentina -Andes Centrales). Estud. Geológicos 43, 345 –358.

Seggiaro, R, Guzmán, S., Martí, J., Montero-López, C., López, E., 2014a. Stratigraphy of the Coranzulí caldera. In: Rocha, R. Pais, J., Kullberg, J. C., Finney, S. (Eds)., Strati 2013: First International Congress on Stratigraphy. At the Cutting Edge of

Stratigraphy: At the cutting edge of stratigraphy. Springer Geology, Cham, pp. 1269–1273.

Seggiaro, R., Guzmán, S., Martí, J., Montero, C., López, E., 2014b. La caldera Coranzulí, Puna Norte. XIX Congreso Geológico Argentino, Córdoba, Argentina, Actas CD-Rom Abstracts: S24-2-5.

Seggiaro, R., Becchio, R. Ramallo, E., Bercheñi, V., 2015. Hoja Geológica 2366-III, Susques (preliminar). Instituto de Geología y Recursos Minerales, Servicio Geológico Minero Argentino, Boletín 414, Buenos Aires.

Soler, M.M., Caffe, P.J., Coira, B.L., Onoe, A.T., Kay, S.M., 2007. Geology of the Vilama caldera: a new interpretation of a large-scale explosive event in the Central Andean plateau during the Upper Miocene. J. Volcanol. Geotherm. Res. 164 (1–2), 23–53. https://doi.org/10.1016/j.jvolgeores.2007.04.

Spray, J. G., 1997. Superfaults. Geology 25, 579– 582.

Suzuki-Kamata, K., Kamata, H., Bacon, C.R., 1993. Evolution of the caldera forming eruption at Crater Lake, Oregon, indicated by component analysis of lithic fragments. J. Geophys. Res. 98, 14059–14074.

Trumbull, R., Riller, U., Oncken, O., Scheuber, E., Munier, K., Hongn, F., 2006. The time-space distribution of Cenozoic arc volcanism in the Central Andes: a new data compilation and some tectonic considerations. In: Oncken, O., Chong, G., Franz, G., Giese, P., Götze, J., Ramos, V., Strecker, M., Wigger, P. (Eds.), The Andes– Active Subduction Orogeny. Frontiers in Earth Science Series 1. Springer- Verlag, Berlin, pp. 29–43.

Walker, G.P.L., 1985. Origin of coarse lithic breccias near ignimbrite source vents. J. Volcanol. Geotherm. Res. 25, 157–171.

Figure captions:

Fig. 1: Location of Miocene calderas and associated deposits in the 21–28°S segment of the Central Volcanic Zone of the Andes. After Petrinovic et al (2010) and Guzmán et al (2017). The inset at the upper right angle is the main figure. The rectangle shows the study area of this contribution.

Fig. 2: Geologic map of the Coranzulí caldera and surroundings.

Fig. 3: Stratigraphic profiles of the medial and distal facies of the Coranzulí ignimbrites.

Fig. 4: Stratigraphic profiles of the proximal facies of the Coranzulí ignimbrites.

Fig. 5: Different volcanic units in the Coranzulí caldera. The inferred caldera rim, main faults and extension axis, and location of profiles from Figs. 3 and 4 are also shown.

Fig. 6: Field photographs of the Coranzulí ignimbrites: (**a**) poorly welded facies (note the subrounded pumice fragments); (**b**) densely welded facies (note the elongated fiamme in the central part of the photograph); (**c**) co-ignimbrite lag breccia forming the base of the second flow unit (note the abundant dense gray co-magmatic lithic fragments); (**d**) Coranzulí ignimbrites forming a plateau, view from the south; (**e**) well-developed columnar jointing in the third ignimbrite flow unit; (**f**) Cerro Coranzulí resurgent dome and lavas; viewed looking NE; (**g**) the Coranzulí resurgent dome (note the altered ignimbrites at the base and lavas at the top); and (**h**) the normal fault on the western rim of the caldera.

Fig. 7: Microphotographs of the Coranzulí ignimbrites: (**a**) densely welded facies; (**b**) poorly welded facies. The white dashed line outlines the pumice fragments. In (**b**) one pumice makes up the upper portion of the image. Bt: biotite, Pl: plagioclase, Qz: quartz.

Fig. 8. Sketch illustrating the evolution of the Coranzulí caldera-forming eruption. White lines indicate the orientation of the cross sections and red line the caldera rim.

Research highlights

- Coranzulí caldera collapse was tectonically driven 6.6 My ago
- Collapse was not homogeneous and occurred along different sectors of the ring fault
- Collapse occurred early in the eruption during a pulsating boiling-over event
- Co-ignimbrite lag breccias reveal the dynamics of caldera collapse
- 4 crystal-rich dacitic ignimbrites with diverse main lithic fragments were emplaced

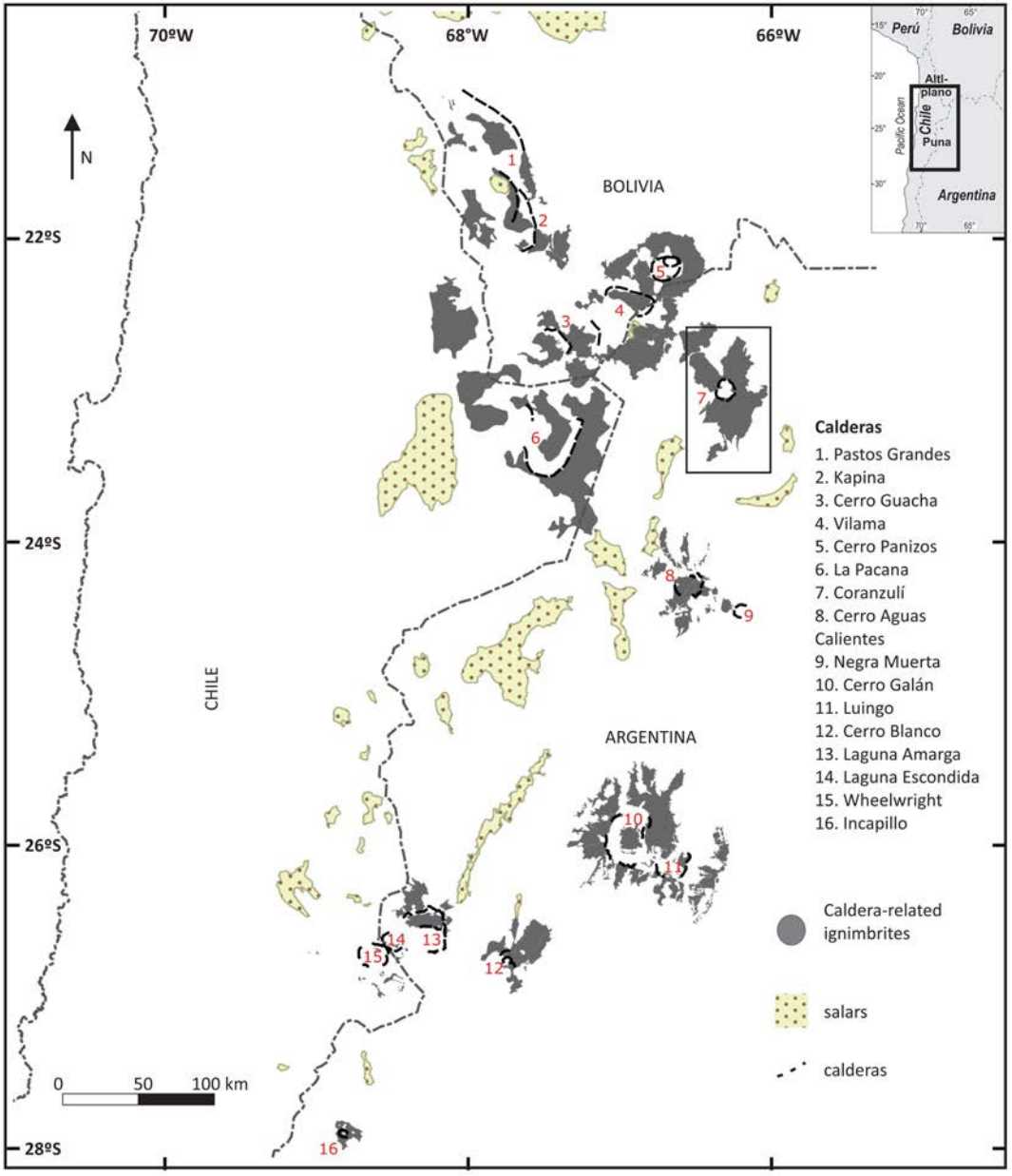

Fig. 1

Figure 1

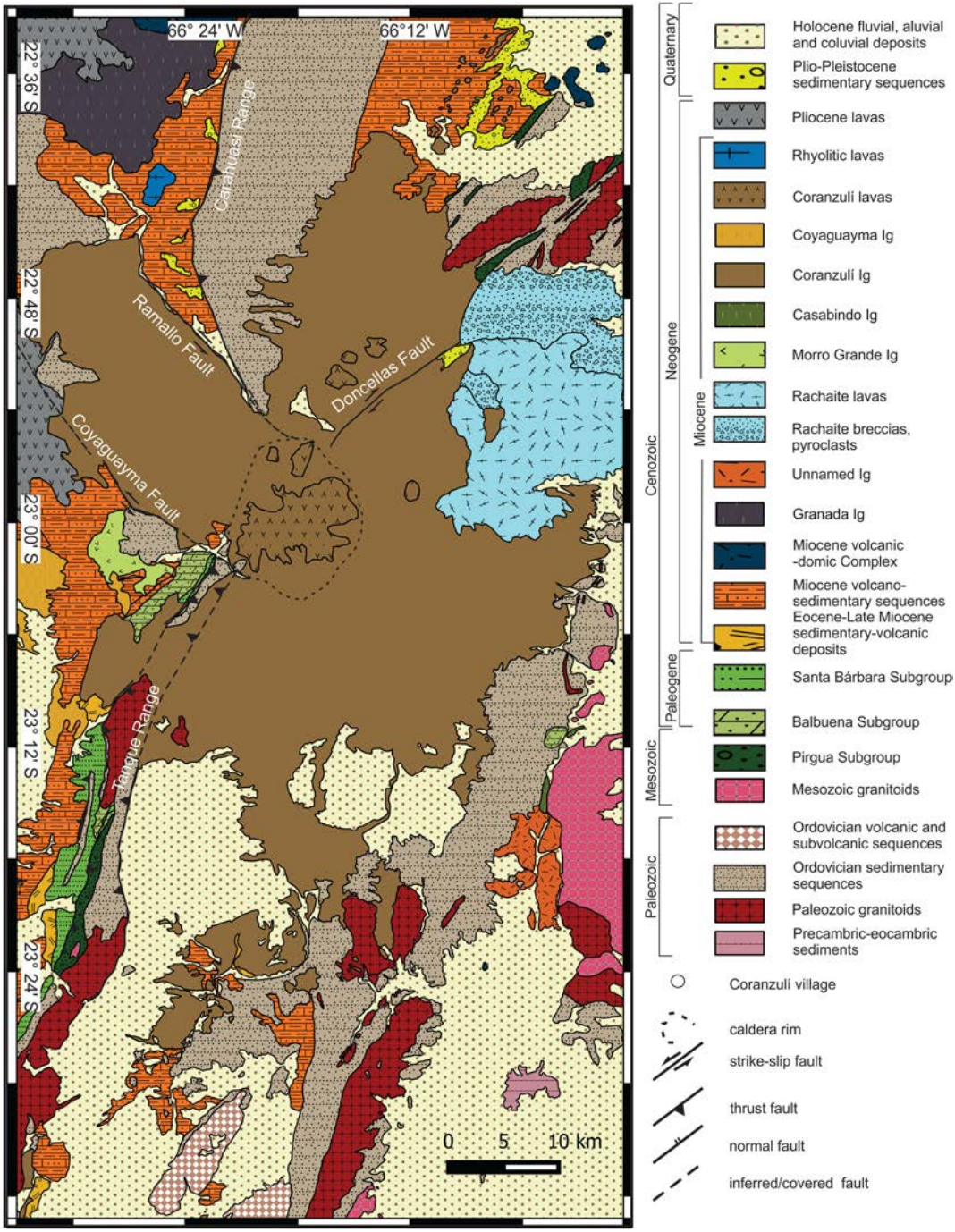
66° 24' W
66°12' W
22° 36' S
22° 48' S
23° 00' S
23° 12' S
23° 24' S
Cazadero Range
Ramallo Fault
Doncellas Fault
Coyaguayma Fault
Tilcara Range
0 5 10 km
Cenozoic
Quaternary
Neogene
Miocene
Paleogene
Mesozoic
Paleozoic
Holocene fluvial, aluvial and coluvial deposits
Plio-Pleistocene sedimentary sequences
Pliocene lavas
Rhyolitic lavas
Coranzulí lavas
Coyaguayma Ig
Coranzulí Ig
Casabindo Ig
Morro Grande Ig
Rachaite lavas
Rachaite breccias, pyroclasts
Unnamed Ig
Granada Ig
Miocene volcanic -domic Complex
Miocene volcano-sedimentary sequences
Eocene-Late Miocene sedimentary-volcanic deposits
Santa Bárbara Subgroup
Balbuena Subgroup
Pirgua Subgroup
Mesozoic granitoids
Ordovician volcanic and subvolcanic sequences
Ordovician sedimentary sequences
Paleozoic granitoids
Precambric-eocambric sediments
Coranzulí village
caldera rim
strike-slip fault
thrust fault
normal fault
inferred/covered fault

Figure 2

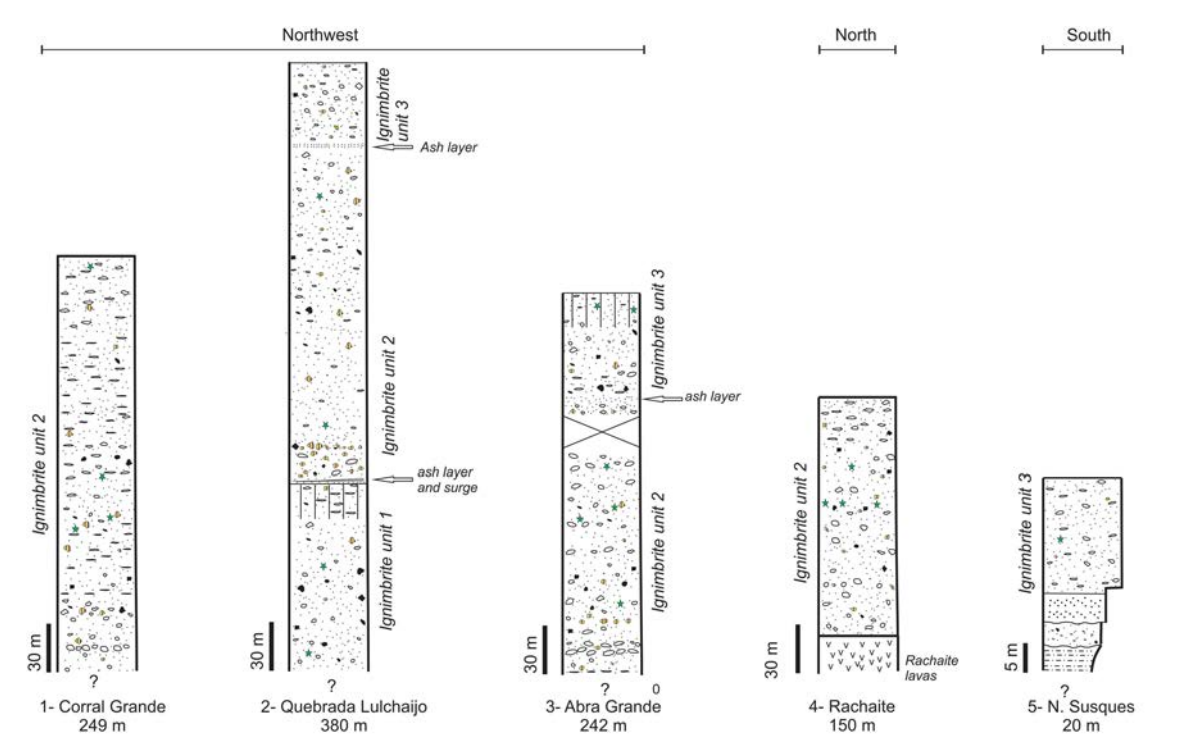
Northwest
North
South
Ignimbrite unit 3
Ash layer
Ignimbrite unit 2
ash layer and surge
Ignimbrite unit 1
Ignimbrite unit 2
30 m
?
1- Corral Grande
249 m
2- Quebrada Lulchaijo
380 m
Ignimbrite unit 3
ash layer
Ignimbrite unit 2
0
3- Abra Grande
242 m
Ignimbrite unit 2
Rachaite lavas
4- Rachaite
150 m
Ignimbrite unit 3
5 m
5- N. Susques
20 m
dense co-magmatic lithic fragments
metamorphic lithics
ordovician lithic fragments
lithics of dacitic lavas
increasing welding degree
pumice and fiamme
columnar joints
covered section

Figure 3

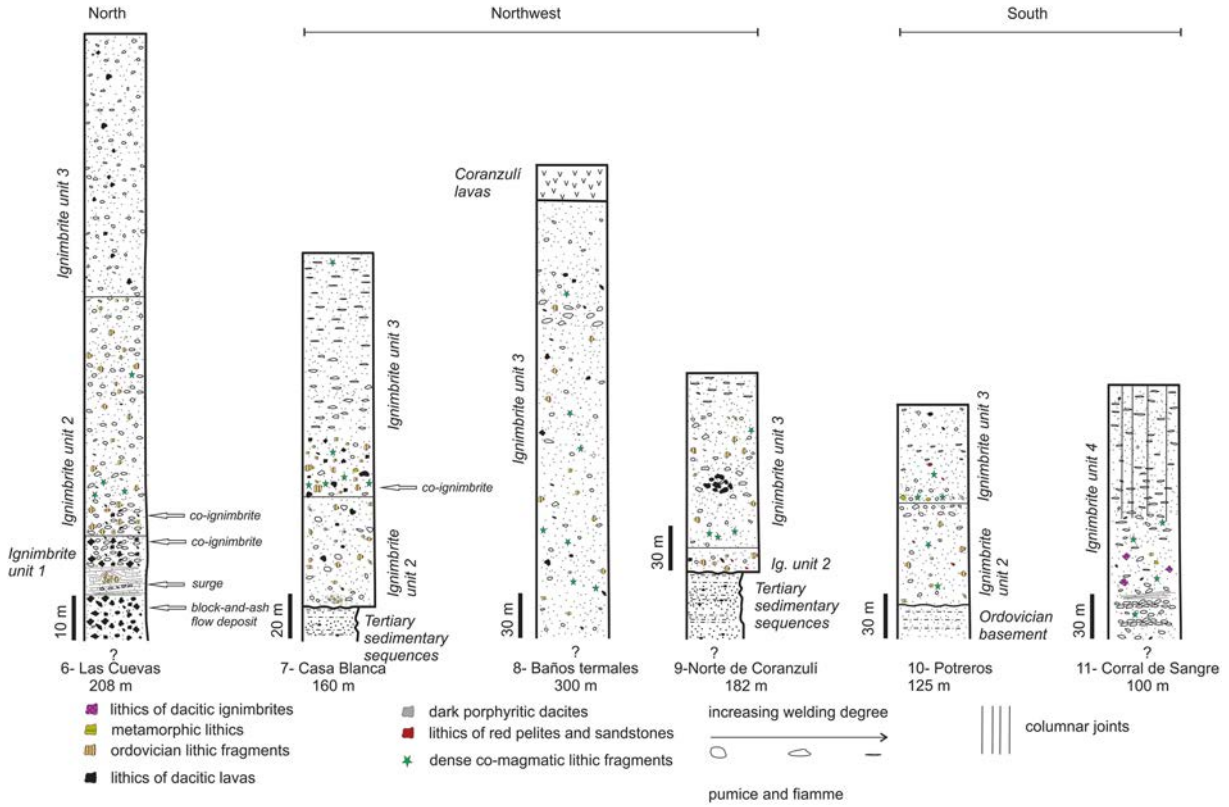
North
Northwest
South
Ignimbrite unit 3
Ignimbrite unit 2
Ignimbrite unit 1
co-ignimbrite
co-ignimbrite
surge
block-and-ash flow deposit
10 m
?
6- Las Cuevas
208 m
Ignimbrite unit 3
co-ignimbrite
Ignimbrite unit 2
20 m
Tertiary sedimentary sequences
?
7- Casa Blanca
160 m
Coranzulí lavas
Ignimbrite unit 3
30 m
?
8- Baños termales
300 m
Ignimbrite unit 3
30 m
lg. unit 2
Tertiary sedimentary sequences
?
9-Norte de Coranzuli
182 m
Ignimbrite unit 3
Ignimbrite unit 2
30 m
Ordovician basement
?
10- Potreros
125 m
Ignimbrite unit 4
30 m
?
11- Corral de Sangre
100 m
lithics of dacitic ignimbrites
metamorphic lithics
ordovician lithic fragments
lithics of dacitic lavas
dark porphyritic dacites
lithics of red pelites and sandstones
dense co-magmatic lithic fragments
increasing welding degree
pumice and fiamme
columnar joints

Figure 4

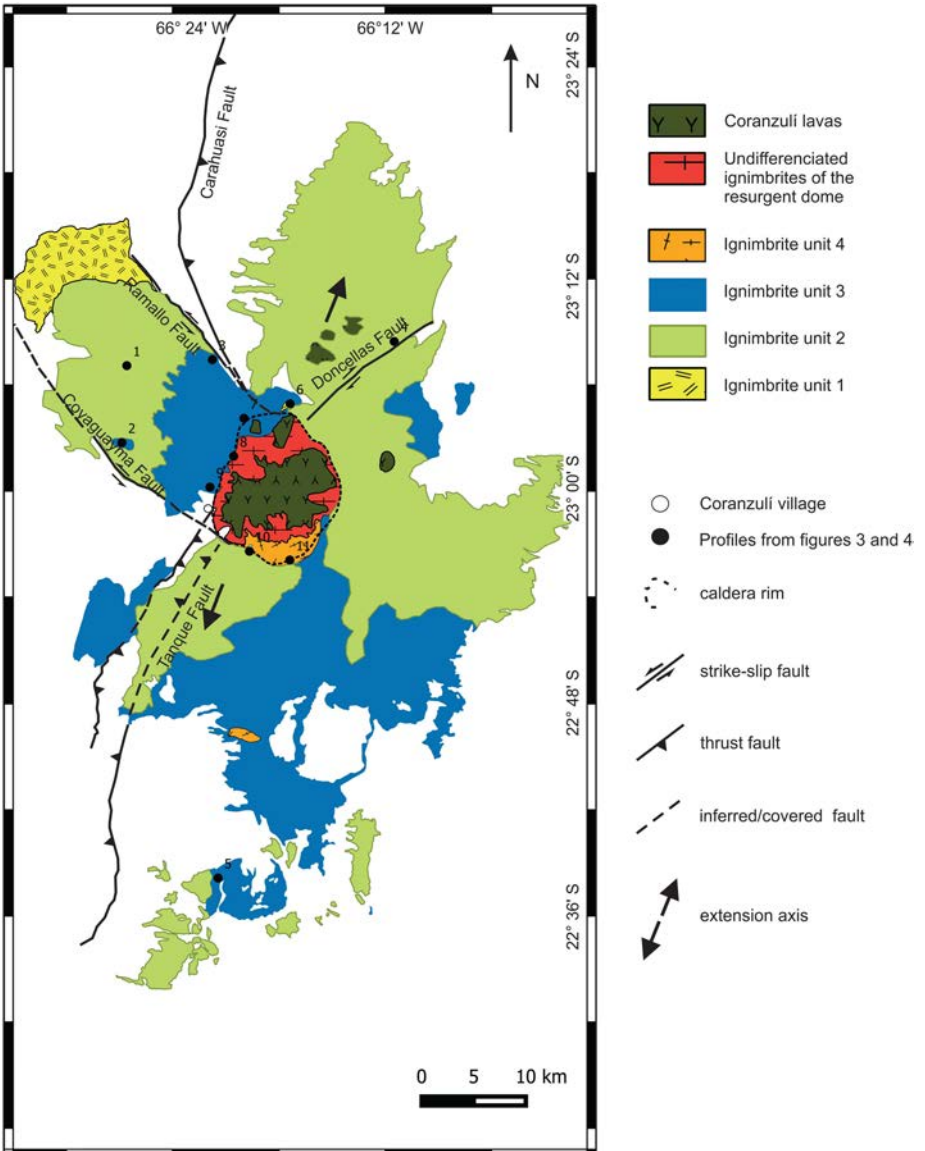
66° 24' W
66°12' W
N
23° 24' S
23° 12' S
23° 00' S
22° 48' S
22° 36' S
Carahuasi Fault
Ramallo Fault
Coyaguayma Fault
Tanque Fault
Doncellas Fault
1
2
3
4
5
6
7
8
9
10
11
12
13
14
0 5 10 km
Coranzuli lavas
Undifferenciated ignimbrites of the resurgent dome
Ignimbrite unit 4
Ignimbrite unit 3
Ignimbrite unit 2
Ignimbrite unit 1
Coranzuli village
Profiles from figures 3 and 4
caldera rim
strike-slip fault
thrust fault
inferred/covered fault
extension axis

Figure 5


pumice
a
fiamme
b
dense
comagmatic
lithic
c
d
e
resurgent dome
f
ENE
WSW
lavas
ignimbrites
g
S
N
h

Figure 6

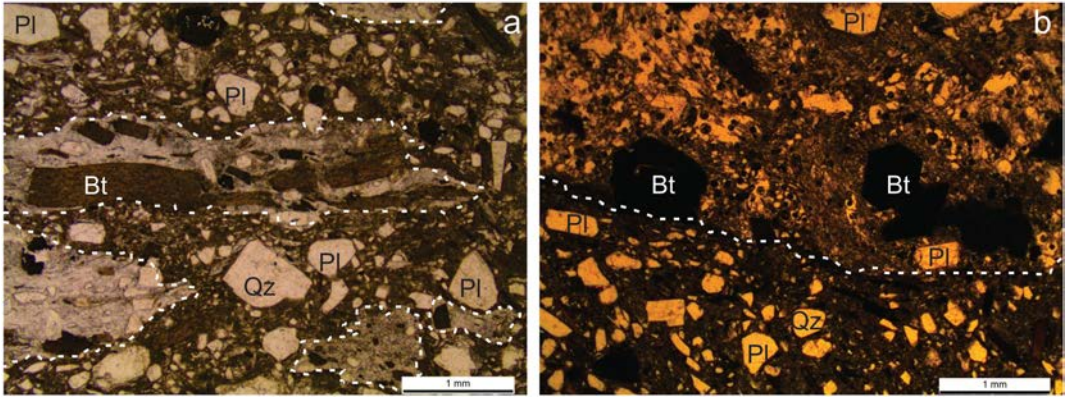

Figure 7

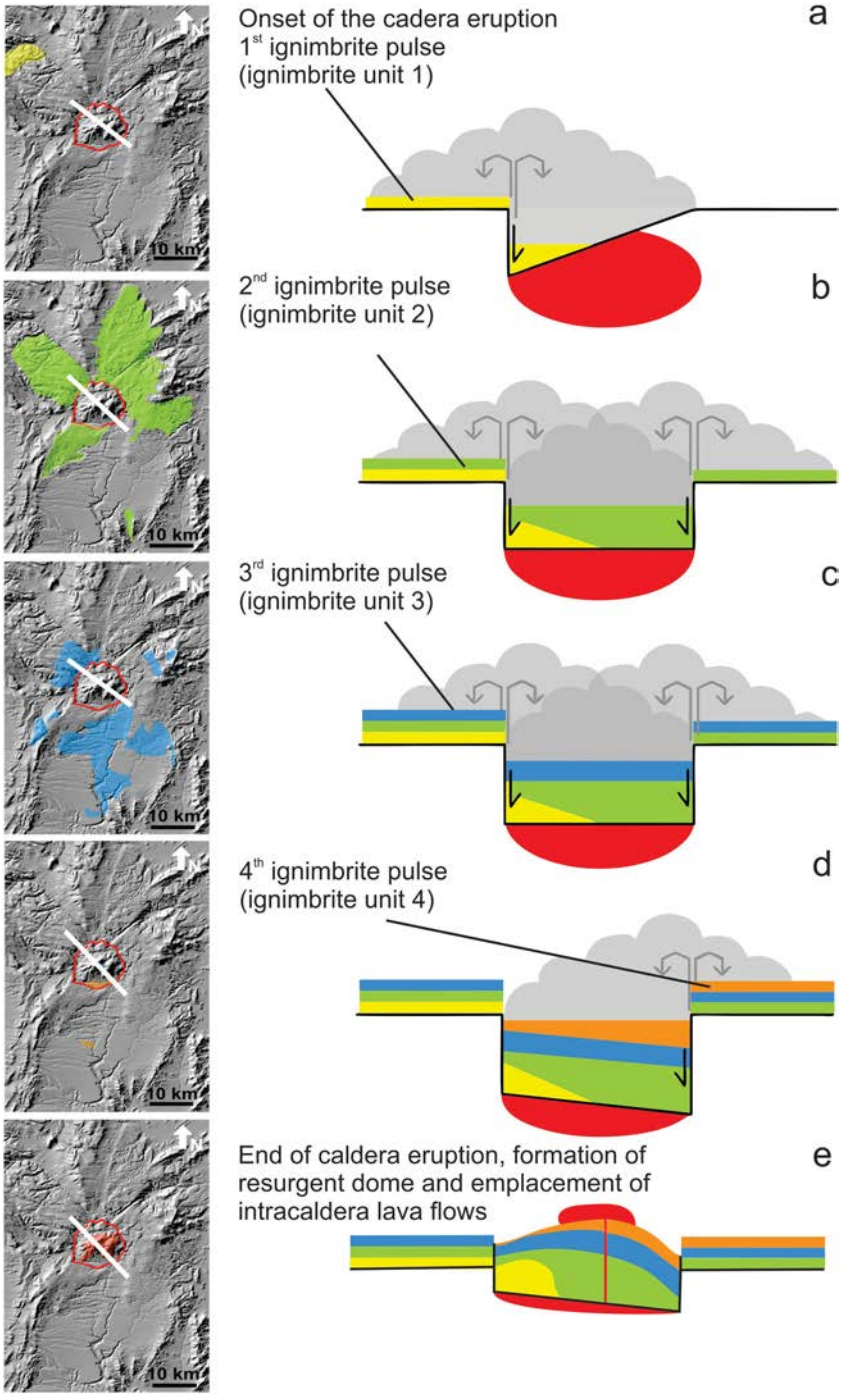
Onset of the cadera eruption
1st ignimbrite pulse
(ignimbrite unit 1)
a
2nd ignimbrite pulse
(ignimbrite unit 2)
b
3rd ignimbrite pulse
(ignimbrite unit 3)
c
4th ignimbrite pulse
(ignimbrite unit 4)
d
End of caldera eruption, formation of
resurgent dome and emplacement of
intracaldera lava flows
e
10 km
N

Figure 8